Self-organization is a dynamic and lineage-intrinsic property of mammary epithelial cells

Lea Chanson[a,1], Douglas Brownfield[b,c,1], James C. Garbe[b], Irene Kuhn[b], Martha R. Stampfer[b], Mina J. Bissell[b,2], and Mark A. LaBarge[b,2]

[a]Institute of Bioengineering, Ecole Polytechnique Fédérale de Lausanne, CH-1015 Lausanne, Switzerland; [b]Life Sciences Division, Lawrence Berkeley National Laboratory, Berkeley, CA 94720; and [c]Department of Bioengineering, University of California, Berkeley, CA 94720

Contributed by Mina J. Bissell, Lawrence Berkeley National Laboratory, December 30, 2010 (sent for review December 6, 2010)

Loss of organization is a principle feature of cancers; therefore it is important to understand how normal adult multilineage tissues, such as bilayered secretory epithelia, establish and maintain their architectures. The self-organization process that drives heterogeneous mixtures of cells to form organized tissues is well studied in embryology and with mammalian cell lines that were abnormal or engineered. Here we used a micropatterning approach that confined cells to a cylindrical geometry combined with an algorithm to quantify changes of cellular distribution over time to measure the ability of different cell types to self-organize relative to each other. Using normal human mammary epithelial cells enriched into pools of the two principal lineages, luminal and myoepithelial cells, we demonstrated that bilayered organization in mammary epithelium was driven mainly by lineage-specific differential E-cadherin expression, but that P-cadherin contributed specifically to organization of the myoepithelial layer. Disruption of the actomyosin network or of adherens junction proteins resulted in either prevention of bilayer formation or loss of preformed bilayers, consistent with continual sampling of the local microenvironment by cadherins. Together these data show that self-organization is an innate and reversible property of communities of normal adult human mammary epithelial cells.

mammary gland | tissue biology

Most mammalian adult tissues are replenished and repaired throughout life by reservoirs of stem cells. As new somatic cells replace old ones or build new tissue, organization and architecture must be maintained. The alternative, loss of organization in adult tissues, is associated with cancer and other diseases. Lineage-specific progenitors or their differentiated progeny must have a means to reach their ultimate site of residence within the adult tissue. The robust ability to organize cells into tissues is marked from conception: Heterogeneous aggregates of dissociated cells from embryonic tissues, suspended in gels or hanging droplets or on agarose-coated plates, self-organize into semblances of the original tissues (1–5). The mechanisms governing self-organization during developmental morphogenesis (6–10) are likely conserved in the maintenance of organization in adult tissues. Here we use normal human mammary epithelial cells (HMEC) as a model to determine how organized states are preserved in normal adult epithelia.

The mammary gland undergoes cycles of proliferation and involution, showing as much as a 10-fold expansion in preparation for lactation followed by return to normal size. During these processes, the precise bilayered branching organization throughout the gland is maintained; secretory luminal epithelial cells (LEPs) line the lumen, surrounded by a layer of contractile myoepithelial cells (MEPs) that are adjacent to the basement membrane. We hypothesized that mammary epithelial cells possessed lineage-specific intrinsic abilities to self-organize into domains of lineage specificity. Such a mechanism would help explain how, for instance, the mammary stem cell-enriched zone in the ducts (11) is maintained separately from the rank-and-file LEPs and MEPs, and how LEPs and MEPs form and maintain bilayers. The phenomenon of self-organization has not been well studied in humans, perhaps because of the challenges of working with primary materials and a paucity of tractable culture systems for maintaining cell types from normal adult tissues. To facilitate a quantitative understanding of those processes in an adult epithelial tissue, we used a robust cell culture system that enables culture of pre-stasis normal HMEC obtained from reduction mammoplasties for 40–60 population doublings while maintaining both the LEP and MEP lineages (12). Flow cytometry-enriched cells from both lineages were placed in arrays of micropatterned microwells, where their distributions were tracked over time to generate a dynamic understanding of lineage-specific self-organizing behavior.

Results and Discussion

Quantification of Self-Organizing Activity in Different Lineages of Normal Human Mammary Epithelial Cells. We first used a classical self-organization assay to determine whether different lineages of cultured HMEC derived from reduction mammoplasty possessed an intrinsic ability to form bilayered structures. Subpopulations of LEPs and MEPs, defined as $CD227^+/CD10^-$/keratin 19 $(K19)^+$/keratin 14 $(K14)^-$ and $CD227^-/CD10^+/K19^-/K14^+$, respectively (11), were enriched by FACS from heterogeneous normal finite-lifespan HMEC (12) at passage 4 or 5 (Fig. 1 *A*, *A′*, and *A″*). The two lineages were labeled with long-lasting fluorescent membrane dyes of different wavelengths, mixed together, and then were suspended in hanging droplets. The formation of cores of LEPs surrounded by MEPs (Fig. 1*B*), similar to their organization in vivo, was observed over 48 h. However, the considerable variation in aggregate size, shape, and focal planes precluded a quantitative understanding of the phenomenon.

Therefore, a microwell culture platform was engineered that confined the HMEC mixtures to a 3D cylindrical geometry, which enabled quantification of lineage distributions over time (Fig. 1*C*). Representative optical sections of mixed LEPs and MEPs in microwells, taken at middepth (~25 μm) at 0 and 48 h, suggest self-organization had occurred, as compared with mixtures of arbitrarily labeled HMEC cultures (Fig. 1*D*). Time-lapse microscopy from one well demonstrates the dynamic nature of the organizing process (Fig. S1 and Movie S1). Heat maps showing the lineage distributions over time suggested that in a majority of microwells MEPs formed a ring surrounding cores of LEPs as early as 24 h, and lasted for at least 48 h (Fig. 1*E*, *Upper*). A 1:1 ratio of LEPs to MEPs was determined empirically to provide the most clearly separable distributions, as compared with ratios of 1:2 or 1:3. Using relatively more LEPs than MEPs (e.g., in a ratio of 2:1 or 3:1) was difficult due to the paucity of LEPs. Arbitrarily labeled HMEC cultures, mixed at a 1:1 ratio, showed overlapping dis-

Author contributions: M.J.B. and M.A.L. designed research; L.C., D.B., J.C.G., and M.A.L. performed research; J.C.G., M.R.S., M.J.B., and M.A.L. contributed new reagents/analytic tools; L.C., I.K., M.R.S., M.J.B., and M.A.L. analyzed data; and I.K., M.J.B., and M.A.L. wrote the paper.

The authors declare no conflict of interest.

[1]L.C. and D.B. contributed equally to this work.

[2]To whom correspondence may be addressed. E-mail: mjbissell@lbl.gov or MALabarge@lbl.gov.

This article contains supporting information online at www.pnas.org/lookup/suppl/doi:10.1073/pnas.1019556108/-/DCSupplemental.

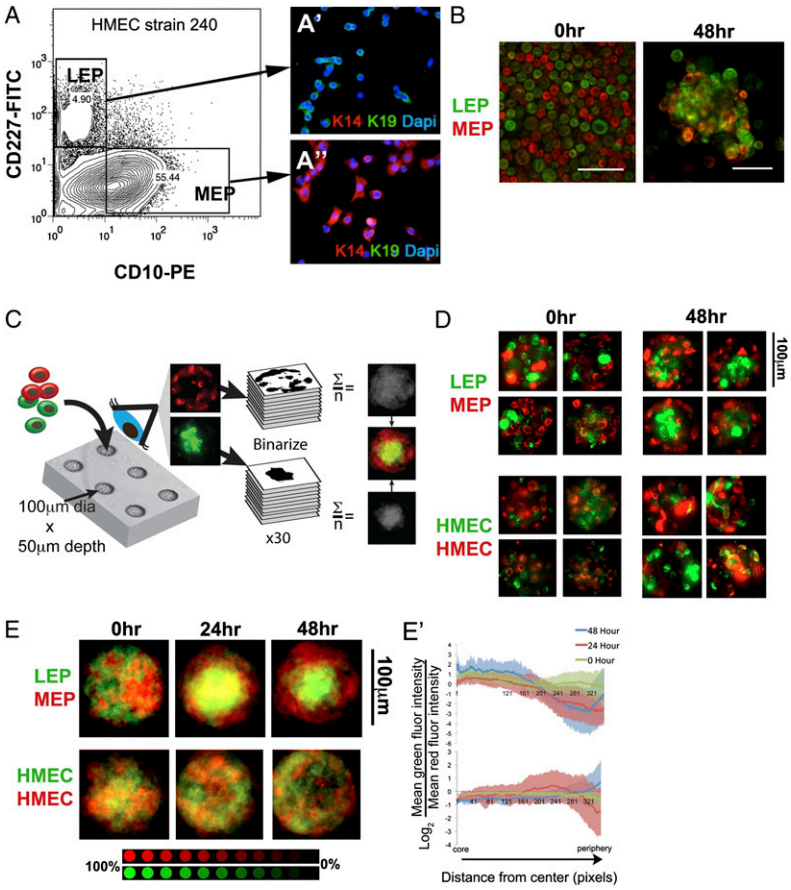

Fig. 1. Heterogeneous mixtures of luminal and myoepithelial cells self-organize into ordered structures. (*A*) Flow cytometry analysis of fourth-passage finite-lifespan HMEC strain 240L reveals distinct populations of the two principal somatic epithelial lineages of mammary gland: MEPs, defined here as $CD227^{-}/CD10^{+}$, and LEPs, defined as $CD227^{+}/CD10^{-}$. (*A′* and *A″*) Immunofluorescence of sorted cells for MEP and LEP markers K14 (red) and K19 (green), respectively, verified that (*A′*) $CD227^{+}$ LEPs were $K14^{-}/K19^{+}$, and (*A″*) $CD10^{+}$ MEPs were $K14^{+}/K19^{-}$. Nuclei were counterstained with DAPI (blue). (*B*) Images of mixtures of fluorescently labeled LEPs (green) and MEPs (red) suspended in hanging droplets and imaged with a confocal microscope just after mixing at 0 h (*Left*) and at 48 h (*Right*). (Scale bars: 20 μm.) (*C*) Cartoon representation of the microwell self-organization assay. Fluorescently labeled LEPs (green) and MEPs (red) were mixed together and placed in arrays of microwells that did not support cell adhesion. Thirty wells were imaged with a confocal microscope just after the addition of cells (0 h) and again at 24 h and 48 h. Fluorescence from both green and red channels in one optical section per well was binarized and then combined and averaged to generate two gray-scale composite images that were overlaid to generate a single two-color composite distribution map for each condition, with LEP distributions in green and MEP distributions in red. (*D*) Representative fluorescence images ofLEP (green) and MEP (red) in four different microwells at 0 h and 48 h (*Upper*) and of controls, which were heterogeneous HMEC arbitrarily labeled with red or green fluorescent labels (*Lower*). (*E*) Distribution maps of LEP (green) and MEP (red) (*Upper*) or control mixtures at the 0-h, 24-h, and 48-h time points (*Lower*). (*E′*) Quantification of heat maps in *E* showing changes in mean distribution of red and green pixels along the radius around 360° of arc at three time points. Green lines show 0 h, red lines show 24 h, and blue lines show 48 h. SD is shown by the lightly shaded regions of colors corresponding to each line.

tributions of cells that did not resolve into distinct populations (Fig. 1*E*, *Lower*). Quantification of the heat maps (Fig S2) confirmed that a core of LEPs surrounded by MEPs was observable as early as 24 h, and showing as much as a fourfold difference in LEP:MEP ratios at the core versus the periphery by 48 h ($P < 0.001$) (Fig. 1*E′*, *Upper*). By contrast there was no difference in ratios at the core and the periphery of the arbitrarily labeled HMEC controls at any time point (Fig. 1*E′*, *Lower*). Inflections in the graphs sometimes were observed toward the peripheral regions because of imperfect registration of the well images. Taken together, these results indicate that self-organizing is an innate property of the LEP and MEP HMEC lineages.

Levels of E-Cadherin Expression Are Lineage Specific. Self-organizing behavior has been ascribed to disparate adhesive properties among the participating cells in embryonic progenitors from the three germ layers, in cancer cell lines, and in fibroblasts engineered to express cell–cell adhesion molecules (the differential adhesion hypothesis, reviewed in ref. 6). Cadherin cell–cell adhesion molecules, particularly E-cadherin, play key roles in tissue morphogenesis during vertebrate gastrulation (13). Quantification of images of fluorescently immunostained tissue sections of normal mammary gland (Fig. 2*A*) from two individuals revealed that more E-cadherin protein was present at the borders between two LEPs than at the borders between a LEP and a MEP ($P < 0.001$) (Fig. 2*B*). Flow cytometry measurements of E-cadherin surface protein levels were made on LEPs and MEPs. In HMEC strains at fourth passage from six individuals, a reproducible pattern was observed, whereby more E-cadherin was detected on LEPs than on MEPs (Fig. 2*C*). The lineage-specific expression levels of E-cadherin made it an attractive candidate for further testing of the differential adhesion hypothesis as it pertains to self-organization among HMEC.

Functional Identification of Adhesion Molecules That Drive Tissue Self-Organization. To determine whether cadherins played a functional role in the self-organization of LEPs and MEPs, inhibitors of E-, P-, and VE-cadherin were added to the medium of the microwell assay to antagonize those specific cell–cell interactions. P-cadherin is expressed by MEPs in vivo but not by LEPs (14). VE-cadherin is expressed by endothelial cells but not by epithelial cells (13) and was used as a control for potential effects of heterotypic cadherin interactions (9). Each of the putative inhibitors was added at the beginning of the experiment and was refreshed every 24 h with medium changes. An antibody that blocked E-cadherin, and recombinant E-cadherin fused to the human IgG-Fc region (recEcad), prevented self-organizing of LEPs and MEPs. Quantification of the heat maps did not reveal differences in LEP:MEP ratios at the core and periphery (Fig. 3 *A* and *A′*). An antibody that blocked P-cadherin did not abolish sorting, because a core enriched for LEPs was surrounded by MEPs ($P < 0.001$) (Fig. 3 *A* and *A′*). However, quantification revealed that there were more MEP at the core [hovering around a ratio of 1:1 (Fig. 3 *A′*)] than in untreated LEPs and MEPs, which usually showed about a twofold enrichment of LEPs at the core (Fig. 1 *E* and *E′*, *Upper*). Those data suggest that LEPs organization at the core is unaffected by P-cadherin antibodies, whereas the MEPs were relatively more challenged in their journey to the periphery. Recombinant VE-cadherin IgG-fusion protein (recVEcad) did not prevent organizing (Fig. 3 *A* and *A′*). These data suggested that differential levels of E-cadherin at the surfaces of LEPs and MEPs were the principle drivers of self-organization and thus were the focus of the majority of subsequent studies. However, these data also show that P-cadherin plays a more lineage-restricted role in MEP self-organizing.

Self-Organization Was Prevented After Negative Modulation of the Actomyosin Network. Previous studies of mammary epithelial morphogenesis have implicated profound roles for the actomy-

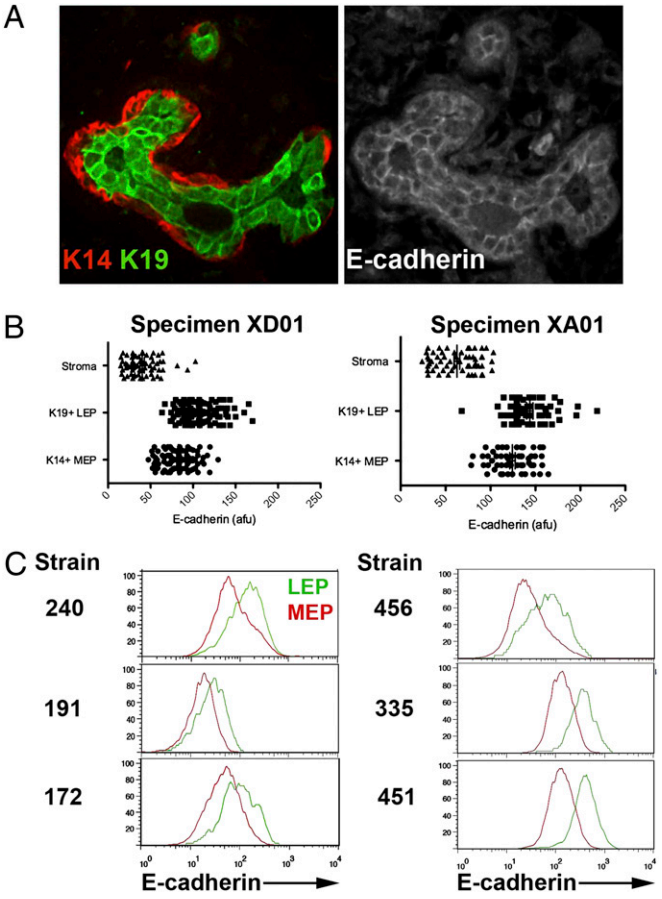

Fig. 2. Epithelial lineages that comprise the mammary gland express E-cadherin differentially. (*A*) A tissue section from a normal mammary gland, specimen XD01, embedded in paraffin and triple-immunostained to show expression of (*Left*) the MEP and LEP markers K14 (red) and K19 (green), respectively, and (*Right*) E-cadherin (gray scale). (*B*) Dot plots show image quantification from two individuals, XD01 and XA01, of E-cadherin protein levels at the border between two LEPs (K19+ LEP) and at the border between an LEP and an MEP cell (K14+ LEP) and background fluorescence as measured on stroma, which does not express E-cadherin (Stroma). Measurements are expressed in arbitrary fluorescence units (afu), n = 100 for each cell type collected from at least three sections. (*C*) Flow cytometry analysis of E-cadherin expression in $CD10^+$ MEPs and $CD227^+$ LEPs in HMEC strains at fourth or fifth passage from six individuals.

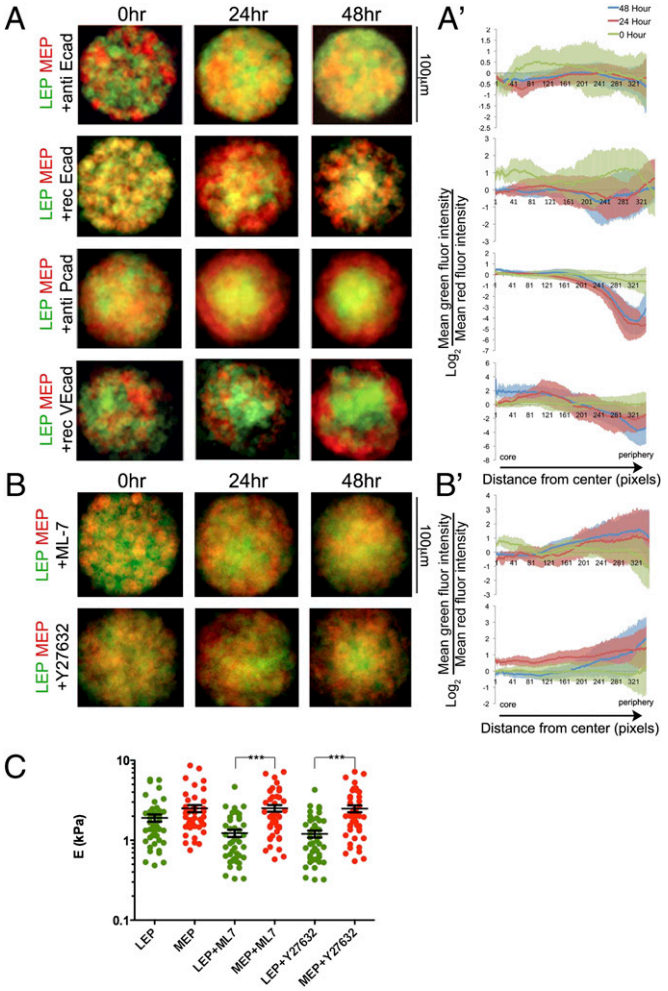

Fig. 3. E-cadherin–containing junctions and the cytoskeleton regulatory molecules ROCK and MLCK are required for self-organizing. (*A*) Maps of HMEC lineage distributions over time in the presence of E-, P-, or VE-cadherin–blocking agents (anti–E-cadherin, recombinant (rec)E-cadherin, anti–P-cadherin, or recVE-cadherin); LEP are green, and MEP are red. (*B*) LEP (green) and MEP (red) distributions in the presence of the MLCK inhibitor ML-7 or the ROCK inhibitor Y27632. (*A′* and *B′*) Quantification of heat maps in *A* and *B*, respectively, showing changes in mean distribution of red (MEP) and green (LEP) pixels along the radius around 360° of arc at three time points. Green lines show 0 h, red lines show 24 h, and blue lines show 48 h. SD is shown by the lightly shaded region of color corresponding to each line. (*C*) Atomic force microscopy measurements of LEP and MEP in the presence of ML-7 and Y27632. The graph represents elasticity (kPa) values for 45 cells per condition; the interior line represents mean elasticity values; error bars show SE. Strain 240L at fourth passage was used for all experiments.

osin regulatory network in normal morphogenesis (15, 16). We therefore examined the impact on HMEC self-organization of the actomyosin network inhibitors ML-7, a myosin light-chain kinase (MLCK) inhibitor (17), and Y27632, a Rho kinase (ROCK) inhibitor that blocks both ROCK1 and ROCK2 (18). Inhibitors were added at the beginning of the experiment and were refreshed every 24 h with medium changes. Analysis of LEPs and MEPs distributions over 48 h revealed that both inhibitors prevented self-organization; there were no differences in lineage distribution between the core and peripheral regions (Fig. 3 *B* and *B′*). Modulation of the actomyosin network also is known to cause changes in the elasticity and cortical tension of cells. Self-organization studies of germline progenitor cells dissociated from zebra fish embryos suggested that differential actomyosin-dependent cell-cortex tension was a crucial component of self-organization in that system (8). Stiffer cells organized to the inside and were surrounded by softer cells, and disruption of the stiffness relationship by actomyosin network inhibitors led to deficits in self-organization (8). Using an atomic force microscope, we measured the elasticity of untreated and inhibitor-treated MEPs and LEPs. Although untreated MEPs tended to be stiffer than LEPs, that difference became significant only in the presence of the inhibitors ($P < 0.001$) (Fig. 3*C*). MEP stiffness was unaffected by ML-7 and by Y27632, but those inhibitors caused softening of LEPs (Fig. 3*C*). In HMEC the actomyosin network inhibitors increased the magnitude of the difference in elasticity between LEPs and MEPs but did not alter their relative elasticity (i.e., LEPs always were softer than MEPs), suggesting that in this system self-organization was not driven by differential elasticity.

Perturbations of the Actomyosin Network in the Microwell Platform Revealed That Self-Organization Is Dynamic and Reversible. How did the actomyosin inhibitors upset the self-organizing mechanism? We investigated whether the actomyosin inhibitors affected expression or binding activities of E-cadherin in HMEC. Addition

of ML-7 or Y27632 to the HMEC culture medium did not change lineage-specific differences in E-cadherin expression as measured via flow cytometry; invariably, LEPs expressed more E-cadherin than did MEPs (Fig. 4*A*). The ability of rec-Ecad simply to bind surfaces of HMEC in suspension also was measured by flow cytometry. Binding of recEcad did not occur in Ca^{2+}-free medium or when HMEC were preincubated with an E-cadherin–blocking antibody (Fig. 4*B*). A 6-h pretreatment with Y27632 or ML-7 did not prevent recEcad binding (Fig. 4*B*). Therefore, neither differential expression levels of E-cadherin nor its ability simply to bind other E-cadherin molecules at the surface was impacted by ML-7 or Y27632.

Because of the central importance of the cytoskeleton in adherens junction regulation, we considered the possibility that the actomyosin inhibitors modulated the ability of E-cadherin junctions to mature or remodel (19), thereby impacting HMEC organization. Disruption of MLCK would prevent proper localization of myosin IIA to the E-cadherin junction, disrupting E-cadherin clustering and decreasing homophilic adhesion (20). Conversely, mature adherens junctions were unable to break down and recycle in the presence of Y27632 in HCT116 and MDCK epithelial cell lines (21). Those reports predicted that ML-7 would ablate already-organized HMEC structures, whereas Y27632 would preserve them. Accordingly, ML-7 or Y27632 was added to mixtures of LEPs and MEPs in the microwell assay, either just after cells were added to wells at the start of the assay (0 h) or after 24 h, when the DMSO controls already started to show signs of organization. In contrast to the experiments shown in Fig. 3*B*, in which the inhibitors were refreshed every 24 h, in these experiments the inhibitors were added a single time, with the expectation, based on empirical findings, that the inhibitor's activity would begin to weaken by 48 h. This protocol tested the reversibility of the system, because in one condition sorting would be prevented from the beginning and then gradually would be unleashed, and in the second condition sorting would be allowed to get underway before perturbation by the inhibitors after 24 h. Both inhibitors, when added at 0 h, prevented self-organization through the 24-h time point, but as the inhibitors' activity diminished significant, differences in LEP:MEP ratios in the core and at the periphery were observed by 48 h ($P < 0.01$) (Fig. 4 *C* and *C′*). The unique phenotypes of each inhibitor were revealed when they were added after the assay had been underway for 24 h. Before addition of the inhibitors, the LEP were enriched at the core and were surrounded by peripheral MEPs ($P < 0.001$) (Fig. 4 *C* and *C′*). When measured at 48 h, addition of ML-7 had obliterated organization, eliminating any difference in the distributions of the lineages (P = ns), whereas Y27632 had preserved the self-organized LEP cores that were encircled by MEPs ($P < 0.001$) (Fig. 4 *C* and *C′*). As a whole, these observations are consistent with the following model: ML-7 prevented adherens junction formation or maturation, and breaking the adherens junctions prevented cells from self-organizing and caused dissolution of already organized structures. Conversely, Y27632 prevented adherens junction recycling, so the cells could not let go of

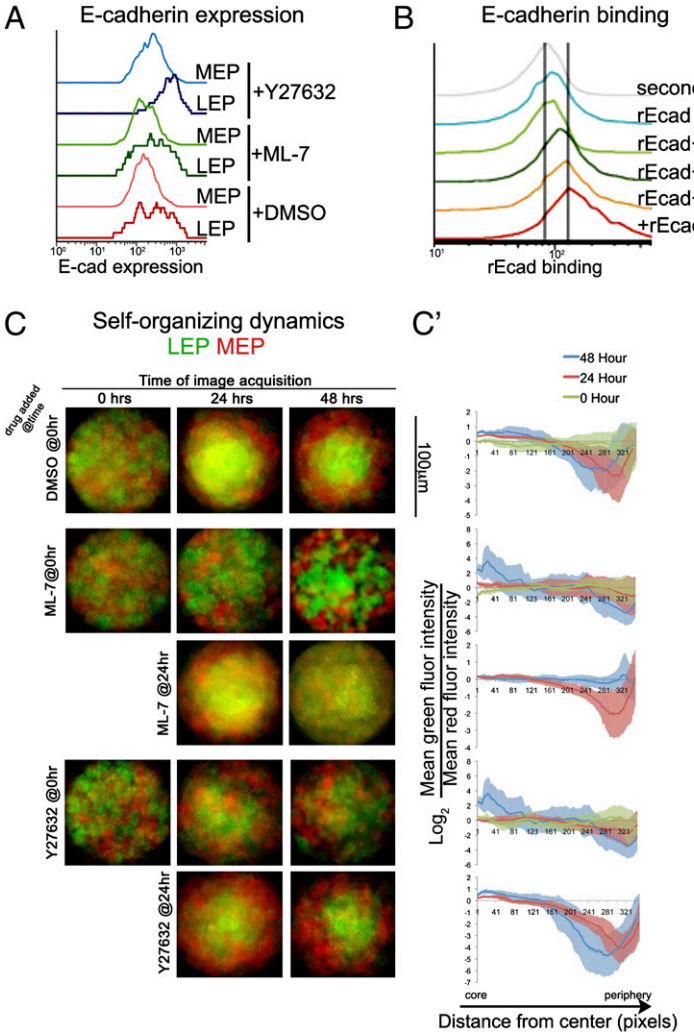

Fig. 4. Self-organization among luminal and myoepithelial cells is driven by E-cadherin activity. (*A*) E-cadherin protein expression at the surface of LEPs and MEPs in the presence of ML-7 or Y27632, as measured by flow cytometry. (*B*) Flow cytometry analysis of recombinant E-cadherin (rEcad) binding to HMEC cell surfaces. (*C*) LEP (green) and MEP (red) distribution maps showing the impact on self-organization over time (time points: 0 h, 24 h, and 48 h) when the inhibitors ML7 and Y27632 were added at 0 h or after 24 h. (*C′*) Quantification of heat maps in *C* showing changes in mean distribution of red (MEP) and green (LEP) pixels along the radius around 360° of arc at three time points: green lines show 0 h, red lines show 24 h, and blue lines show 48 h. SD is shown by the lightly shaded region of color corresponding to each line. Strain 240L at fourth passage was used for all experiments.

CELL BIOLOGY

one another to sample the surrounding microenvironment. Thus, both establishing and maintaining organized states are dynamic and reversible processes.

Here we demonstrated that self-organization of mammary epithelial cells is a lineage-specific process that is principally E-cadherin driven; however, P-cadherin also may play a role in organizing the MEP layer. Unaltered normal finite-lifespan HMEC and the microwell assay were used together with recombinant proteins and antibodies that blocked specific adherens junction proteins. The elegant proof-of-principal experiments, which that showed differential levels of cell–cell adhesion molecules can drive self-organizing, were performed using fibroblasts and other immortal cell lines that were engineered to express different levels of adherens junction proteins. It is remarkable, given the undoubted complexity of the LEP and MEP cell surfaces, that E-cadherin plays so central a role in the process of self-organization in those cells. It has been hypothesized that self-organizing is not simply the result of differential levels of cadherin expression or of binding affinities, but rather that adhesion energy and the ability to remodel cell–cell junctions are crucial determinants (22). Dynamic analysis of HMEC in the microwell assay platform in the presence of actomyosin inhibitors provided support for that hypothesis in the context of mammary gland (Fig. 4 *C*–*C′*). Elegant time-lapse imaging studies of mouse mammary organoid morphogenesis also revealed that the actomyosin inhibitors Y27632 and ML-7 disrupted the clean bilayered organization (15), but not to the catastrophic extent observed in the HMEC microwell assay. Because the mouse mammary organoids were developed in vivo, a number of additional cellular interconnectivities crucial for tissue stability may have formed that were absent in our recombined system. Although we focused on cell–cell E-cadherin junctions, other adhesive and physical interactions, such as desmosomal interactions between LEPs and MEPs (23), undoubtedly are important in maintaining mammary gland organization and bear further dissection. Cell–extracellular matrix (ECM) interactions also will likely affect sorting in vivo. Because the microwell assay uses a nonfouling coating to prevent cell adhesion, the adherens junction proteins may have had a more pronounced effect on self-organizing than they would have had in the presence of ECM. Atomic force microscopy analysis of LEP and MEP on plastic dishes indicated that LEP tended to be softer than MEP. However, a cultured murine epithelial cell line became less stiff in contact with laminin-111, a principal component of basement membrane, than when in contact with plastic (24). Therefore, MEPs in vivo may be less or equally as stiff as LEPs because of their direct contact with basement membrane. Future iterations of the microwell platform will help elucidate more of the factors involved in making stable and organized tissues.

Studying self-organizing behavior of a human epithelium generally is challenging because results cannot be extrapolated easily to in vivo conditions. However, observations of breast cancer pathogenesis suggest the basic mechanisms described here are important for maintaining mammary gland organization. E-cadherin expression and localization frequently are misregulated in breast cancers (25–27), and loss of E-cadherin is a hallmark of the epithelial-to-mesenchymal transition, which is associated with invasive and aggressive breast cancer (28). The mechanisms governing self-organization also are important in the context of regenerative tissue maintenance. As MEPs and LEPs are produced anew by mammary progenitor cells in vivo, they must adopt their appropriate place within the tissue, or, alternatively, the progenitors must be able to move to receive instructive microenvironments that direct cell-fate decisions (29). Understanding tissue self-organization mechanisms may help explain how stem cell differentiation and maintenance of tissue architecture in adults are coordinated.

Materials and Methods

Cell Culture. HMEC strains were established and maintained according to previously reported methods (12, 30). Cells were maintained in M87A medium and used for assays at fourth and fifth passages; strain 240L was the only strain used for self-organizing and binding assays.

Microwell Self-Organization Assay. Micropatterned substrata were made according to Tan et al. (31). Polydimethylsiloxane (PDMS) microwell arrays were formed by curing prepolymer with base:cure ratio of 10:1 (Sylguard 184) against a prepatterned master. The arrays of wells were peeled away and were cut into 1-cm^2 pieces that were affixed with a few microliters of uncured PDMS to the bottom of a 24-well plate (Mitek). Plates with microwells were UV oxidized for 7 min (UVO-Cleaner 42; Jelight Co.), blocked with 2 mg/mL BSA (Sigma) for 1 h under vacuum, and rinsed with PBS and M87A. All self-organizing experiments were conducted with HMEC strain 240L. Flow cytometry-sorted HMEC were stained with CM-DiI, SP-DiOC18 (3), or DiIC18(5)-DS (Invitrogen), used at 1:1,000 in PBS for 5 min at 37 °C followed by 15 min at 4 °C. Cells were washed extensively with medium after staining. Dye-stained HMEC were mixed at a ratio of 1:1 (LEP:MEP) or 1:1 (randomly stained green:red HMEC cultures) and were resuspended in M87A at 1 million cells/mL. Inhibitors were added to the cell suspensions just before HMEC were introduced into the wells and were allowed to load for 30–60 min. Excess cells were washed away with medium; inhibitors then were added to the medium after excess cells were washed away and at every medium change. anti–E-cadherin (100 μg/mL clone HECD-1; Invitrogen); anti–E-cadherin (100 μg/mL clone HECD-1; Invitrogen); anti–P-cadherin (100 μg/mL clone NCC-CAD-299; Abcam); recombinant human (rh)E-cadherin-Fc (recEcad, 100 μg/mL; R&D Systems); rhVE-cadherin (100 μg/mL; R&D Systems); Y27632 (10^{-5} M; Calbiochem); or ML-7 at 3×10^{-6} M (Calbiochem). HMEC were imaged at 0, 24, or 48 h with a spinning disk confocal microscope (Carl Zeiss). Red and green fluorescence channels in images taken at the ~25-μm *z* axis positions of 30 wells from each condition at each time point were binarized using the Threshold function, merged into a Z-stack, and then averaged using ImageJ software (National Institutes of Health). Gray-scaled average images corresponding to LEP and MEP were merged into a single image with red or green look-up tables applied to each average image.

Heat maps were normalized to the highest intensity value and were used to quantify sorting using the expression $\log_2$(mean green pixel intensity/mean red pixel intensity). A script was written using MATLAB (Mathworks) to plot differential intensity as a function of the distance from the center and to compute the average plot from θ of 0–360° (Fig S2).

Flow Cytometry Sorting and Assays. HMEC at fourth or fifth passage were trypsinized and resuspended in medium. For enrichment of LEP and MEP images, anti–CD227-FITC (clone HMPV; BD) or anti–CD10-PE (clone HI10a; BioLegend) was added to the medium at 1:50 for 25 min on ice. HMEC then were washed in PBS and sorted on a FACS Vantage DIVA (BD) into their own medium.

E-cadherin expression on LEP and MEP was measured by addition of anti–E-cadherin-A647 (clone 67A4; Biolegend) to the above mixture at 1:50.

Atomic Force Microscopy Measurements of Stiffness. Once samples were equilibrated to 25 °C, cell deformity was measured, and stiffness was calculated as previously described (24). The resulting data were plotted using Prism(GraphPad Software) (n = 45).

Statistics. E-cadherin images and atomic force microscopy were analyzed using the Kruskal–Wallis test and Dunn's test for multiple comparisons, using a 95% confidence interval. Differences between first and third thirtiles of $\log_2$ (mean green fluorescence/mean red fluorescence) per pixel plotted as a function of distance from the center were analyzed by one-way ANOVA, using Bartlett's test for equal variance and followed by a Tukey's test for multiple comparison using a 99.9% confidence interval. Statistics were computed with Prism (GraphPad Software, Inc.).

ACKNOWLEDGMENTS. We thank Drs. Matthias Lutolf and Celeste M. Nelson for insightful discussions, Celeste M. Nelson. for providing micropatterned wafers, and Dr. Daniel Fletcher for use of his atomic force microscope. M.A.L is supported by Grant R00AG033176 from the National Institute on Aging, Grant U54CA112970 from the National Cancer Institute, and by Laboratory Directed Research and Development (LDRD) funding from the Lawrence Berkeley National Laboratory, provided by the Director, Office of Science, of the US Department of Energy under Contract DE-AC02-05CH11231. M.J.B. is supported by grants from the US Department of Energy, Office of Biological and Environmental Research, a Distinguished Fellow Award, Low Dose Radiation Program contract DE-AC02-05CH1123; National Cancer Institute Grants R37CA064786, U54CA126552, R01CA057621, U54CA112970, U54CA143836, and U01CA143233; and by US Department of Defense Grant W81XWH0810736. M.R.S. and J.C.G. are supported by US Department of Defense Grants BCRP BC060444 and U54CA112970.

1. Steinberg MS (1962) Mechanism of tissue reconstruction by dissociated cells. II. Time-course of events. *Science* 137:762–763.
2. Steinberg MS (1962) On the mechanism of tissue reconstruction by dissociated cells, Iii. Free energy relations and the reorganization of fused, heteronomic tissue fragments. *Proc Natl Acad Sci USA* 48:1769–1776.
3. Steinberg MS (1962) On the mechanism of tissue reconstruction by dissociated cells. I. Population kinetics, differential adhesiveness, and the absence of directed migration. *Proc Natl Acad Sci USA* 48:1577–1582.
4. Townes PL, Holtfreter J (1955) Directed movements and selective adhesion of embryonic amphibian cells. *J Exp Zool* 128:53–120.
5. Wei C, Larsen M, Hoffman MP, Yamada KM (2007) Self-organization and branching morphogenesis of primary salivary epithelial cells. *Tissue Eng* 13:721–735.
6. Foty RA, Steinberg MS (2004) Cadherin-mediated cell-cell adhesion and tissue segregation in relation to malignancy. *Int J Dev Biol* 48:397–409.
7. Foty RA, Steinberg MS (2005) The differential adhesion hypothesis: A direct evaluation. *Dev Biol* 278:255–263.
8. Krieg M, et al. (2008) Tensile forces govern germ-layer organization in zebrafish. *Nat Cell Biol* 10:429–436.
9. Shi Q, Chien YH, Leckband D (2008) Biophysical properties of cadherin bonds do not predict cell sorting. *J Biol Chem* 283:28454–28463.
10. Manning ML, Foty RA, Steinberg MS, Schoetz EM (2010) Coaction of intercellular adhesion and cortical tension specifies tissue surface tension. *Proc Natl Acad Sci U S A* 107(28):12517–12522.
11. Villadsen R, et al. (2007) Evidence for a stem cell hierarchy in the adult human breast. *J Cell Biol* 177:87–101.
12. Garbe JC, et al. (2009) Molecular distinctions between stasis and telomere attrition senescence barriers shown by long-term culture of normal human mammary epithelial cells. *Cancer Res* 69:7557–7568.
13. Gumbiner BM (2005) Regulation of cadherin-mediated adhesion in morphogenesis. *Nat Rev Mol Cell Biol* 6:622–634.
14. Shimoyama Y, et al. (1989) Cadherin cell-adhesion molecules in human epithelial tissues and carcinomas. *Cancer Res* 49:2128–2133.
15. Ewald AJ, Brenot A, Duong M, Chan BS, Werb Z (2008) Collective epithelial migration and cell rearrangements drive mammary branching morphogenesis. *Dev Cell* 14: 570–581.
16. Vargo-Gogola T, Heckman BM, Gunther EJ, Chodosh LA, Rosen JM (2006) P190-B Rho GTPase-activating protein overexpression disrupts ductal morphogenesis and induces hyperplastic lesions in the developing mammary gland. *Mol Endocrinol* 20: 1391–1405.
17. Makishima M, et al. (1991) Induction of differentiation of human leukemia cells by inhibitors of myosin light chain kinase. *FEBS Lett* 287:175–177.
18. Davies SP, Reddy H, Caivano M, Cohen P (2000) Specificity and mechanism of action of some commonly used protein kinase inhibitors. *Biochem J* 351:95–105.
19. Fukata M, Kaibuchi K (2001) Rho-family GTPases in cadherin-mediated cell-cell adhesion. *Nat Rev Mol Cell Biol* 2:887–897.
20. Smutny M, et al. (2010) Myosin II isoforms identify distinct functional modules that support integrity of the epithelial zonula adherens. *Nat Cell Biol* 12:696–702.
21. Sahai E, Marshall CJ (2002) ROCK and Dia have opposing effects on adherens junctions downstream of Rho. *Nat Cell Biol* 4:408–415.
22. Borghi N, James Nelson W (2009) Intercellular adhesion in morphogenesis: Molecular and biophysical considerations. *Curr Top Dev Biol* 89:1–32.
23. Runswick SK, O'Hare MJ, Jones L, Streuli CH, Garrod DR (2001) Desmosomal adhesion regulates epithelial morphogenesis and cell positioning. *Nat Cell Biol* 3:823–830.
24. Alcaraz J, et al. (2008) Laminin and biomimetic extracellular elasticity enhance functional differentiation in mammary epithelia. *EMBO J* 27:2829–2838.
25. Zhang X, et al. (2009) Atypical E-cadherin expression in cell clusters overlying focally disrupted mammary myoepithelial cell layers: Implications for tumor cell motility and invasion. *Pathol Res Pract* 205:375–385.
26. Korkola JE, et al. (2003) Differentiation of lobular versus ductal breast carcinomas by expression microarray analysis. *Cancer Res* 63:7167–7175.
27. Moll R, Mitze M, Frixen UH, Birchmeier W (1993) Differential loss of E-cadherin expression in infiltrating ductal and lobular breast carcinomas. *Am J Pathol* 143: 1731–1742.
28. Cano A, et al. (2000) The transcription factor snail controls epithelial-mesenchymal transitions by repressing E-cadherin expression. *Nat Cell Biol* 2:76–83.
29. LaBarge MA, et al. (2009) Human mammary progenitor cell fate decisions are products of interactions with combinatorial microenvironments. *Integr Biol* 1:70–79.
30. Stampfer MR, Bartley JC (1985) Induction of transformation and continuous cell lines from normal human mammary epithelial cells after exposure to benzo[a]pyrene. *Proc Natl Acad Sci USA* 82:2394–2398.
31. Tan JL, Liu W, Nelson CM, Raghavan S, Chen CS (2004) Simple approach to micropattern cells on common culture substrates by tuning substrate wettability. *Tissue Eng* 10:865–872.